Stability and Dynamics of Microring Combs: Elliptic function solutions of the Lugiato-Lefever equation

CHANG SUN[1], TRAVIS ASKHAM[2], AND J. NATHAN KUTZ[1,2,*]

[1] Department of Physics, University of Washington, Seattle, WA 90195
[2] Department of Applied Mathematics, University of Washington, Seattle, WA 90195-3925
[*] Corresponding author: kutz@uw.edu

Compiled September 5, 2018

We consider a new class of periodic solutions to the Lugiato-Lefever equations (LLE) that govern the electromagnetic field in a microresonator cavity. Specifically, we rigorously characterize the stability and dynamics of the Jacobi elliptic function solutions of the LLE and show that the dn solution is stabilized by the pumping of the microresonator. In analogy with soliton perturbation theory, we also derive a microcomb perturbation theory that allows one to consider the effects of physically realizable perturbations on the comb line stability, including effects of Raman scattering and stimulated emission. Our results are verified through full numerical simulations of the LLE cavity dynamics. The perturbation theory gives a simple analytic platform for potentially engineering new resonator designs.

OCIS codes: *(140.4780) Optical resonators; (140.3945) Microcavities; (060.5530) Pulse propagation and temporal solitons; (190.0190) Nonlinear optics*

http://dx.doi.org/10.1364/josab.XX.XXXXXX

INTRODUCTION

Frequency comb generation in microresonators has become a critically enabling technology for applications in metrology, high-resolution spectroscopy and microwave photonics [1–8]. A clear goal in such microresonators is the generation of octave-spanning combs, which is often achieved by the generation of a single soliton in a high-Q microresonator cavity [9, 10]. Much like the multi-pulsing instability (MPI) in mode-locked laser cavities [11–13], microresonators are prone to generating multiple pulses in the cavity [14, 15], thus compromising the performance of the frequency comb generation. Consequently, the dynamics and stability of pulse generation in the microresonator is of significant interest. In this manuscript, we explore analytically tractable solutions of the Lugiato-Lefever equation (LLE) [16], which is the governing equation for the microresonator dynamics [17]. While solitons have been observed in a number of experimental architectures, the deterministic manipulation of states with multiple solitons in microresonators has only been recently explored with the goal of prediction and control [14]. We develop a perturbation theory for periodic pulse train solutions, known as Jacobi elliptic functions, which characterize the underlying solutions in the microresonator cavity. Our work provides a theoretically rigorous complement to recent experimental observations for the transitions between N to $N+1$ (or vice versa) pulses in a microresonator. We further show how cavity perturbations, due to, for instance, the Raman effect or spontaneous emission noise, affect the resulting combline stability and robustness.

Soliton perturbation theory has been one of the most successful theoretical tools developed for characterizing the underlying physics in optical communication systems [18–21] and mode-locked lasers [22–25]. In this work, we develop a LLE combline perturbation theory. The theory relies on an analytic solution, the Galilean invariant one-soliton solution, of the nonlinear Schrödinger equation. Jacobi elliptic functions are a generalization of soliton solutions of the LLE equation, capable of representing both single localized pulse solutions and periodic pulse trains. Much like solitons, the solutions are parameterized by a number of free parameters whose slow evolution under perturbation characterizes the stability of the solution. A linear stability analysis of the Jacobi elliptic solutions is capable of revealing key properties of the combline properties under perturbation. Specifically, our analysis characterizes the stability of N pulses per round trip in the laser cavity. Much like MPI in mode-locked lasers [11–13], an initial cavity cold start will jump to the most energetically favorable configuration. However, our analysis shows how one can manipulate the number of pulses per round trip by simply manipulating the microresonator detuning, confirming experimental findings.

From a technical point of view, our stability analysis follows closely the rigorous theory of soliton perturbation theory. For the LLE Jacobi elliptic solutions, the linearized operator contains four zero modes which correspond to invariances of the solu-

tions. The effect of perturbations on these zero modes is quantified and shows how various perturbations can either destabilize the solutions or force solutions to translate or bifurcate to a higher or lower number of pulses per round trip. Additionally, we show that the remainder of the continuous spectrum remains bounded under perturbation. We demonstrate the application of the theory on two canonical examples: (i) the LLE modified to include Raman dynamics, and (ii) the LLE under the influence of white noise (stimulated emission noise) perturbations. In both cases, we show that the comblines remain stable while the solitons undergo translation. Given the tremendous impact that soliton perturbation theory has had on theoretical understanding of light-wave transmission systems, our goal is to provide a similar LLE combline perturbation theory for theoretical characterization of microresonators.

The paper is outlined as follows: In Sec. 2, the LLE is introduced along with the scalings to be used in our perturbation theory. Section 3 gives a brief overview of the perturbation theory to be used for modeling the microresonator. Section 4 and 5 present the Jacobi elliptic function solutions that satisfy the LLE equation and their detailed linear stability analysis respectively. The effects of two canonical perturbations due to Raman and simulated emission are considered in Sec. 6. Section 7 provides a brief summary and outlook for the theoretical method developed.

LUGIATO LEFEVER EQUATION

The Lugiato-Lefever equation (LLE), which was originally derived in the context of detuned cavity resonators [16], has been shown to describe the evolution of the electromagnetic field in microresonators [17]. The LLE is a modification of the nonlinear Schrödinger equation (NLSE) which includes damping, detuning and a driving/pumping term. In dimensionless form, the LLE is given by the partial differential equation (PDE)

$$\frac{\partial u}{\partial t} = -(\epsilon + i\alpha)u + i|u|^2u - i\frac{\beta}{2}\frac{\partial^2 u}{\partial x^2} + \epsilon F + \epsilon G(u,x,t), \quad \textbf{(1)}$$

where $u(x,t)$ the complex envelope of the total intracavity electric field, β determines the microring dispersion ($\beta > 0$ is normal group-velocity dispersion while $\beta < 0$ is anomalous group-velocity dispersion), α is the cavity detuning parameter, F characterizes the external cavity pumping, and $x \in [-\pi, \pi)$ since the microresonator enforces periodic boundary conditions [17]. In our specific scaling, the parameter $\epsilon \ll 1$ is used to model the effects of linear cavity attenuation and small perturbations of the form $G(u,x,t)$ to the dominant balance dynamics of dispersion, Kerr self-phase modulation, and detuning.

In our scalings, the LLE can be written as a perturbed version of the detuned NLSE so that

$$i\frac{\partial u}{\partial t} - \frac{\beta}{2}\frac{\partial^2 u}{\partial x^2} + |u|^2u - \alpha u = i\epsilon(F - u + G(u,x,t)). \quad \textbf{(2)}$$

This scaling allows us to develop a systematic perturbation analysis of previously unconsidered periodic, Jacobi elliptic solutions of the LLE. This complements the detailed stability analysis of Godey et al. [26] which details the onset of a myriad of spatio-temporal patterns in the LLE model. Specifically, they show that the steady-state solutions of the LLE (with all temporal and spatial derivatives set to zero) lead to a host of pattern-forming instabilities [27] that are ultimately responsible for the generation of strongly nonlinear periodic waveforms. In our analysis, we consider the stability of Jacobi elliptic solutions which are strongly nonlinear solutions whose dominant balance includes temporal and spatial derivative terms [28–31].

BACKGROUND: PERTURBATION THEORY

Our stability analysis determines the spectrum of the resulting linearized operator along with the effects of perturbations on the evolution of the solution parameters. In its most general form, we can consider the one dimensional PDE

$$\frac{\partial u}{\partial t} = N(u, u_x, u_{xx}, \cdots, \mu) + \epsilon G(u,x,t)\,, \quad \textbf{(3)}$$

where $N(\cdot)$ represents some nonlinear dynamics (for which an analytical solution is known), $\epsilon G(u,x,t)$ is a perturbation to these dynamics, and μ is a (bifurcation) parameter. A multi-scale perturbation expansion [32, 33] is a representation of the solution of the form

$$u(x,t) = u_0(x,t,\tau) + \epsilon u_1(x,t) + \epsilon^2 u_2(x,t) + \cdots\,, \quad \textbf{(4)}$$

where $\tau = \epsilon t$ corresponds to a slow variable dependence [19, 34].

Collecting terms at each order of ϵ gives nonlinear dynamics for the leading order term and forced, linear dynamics for all other orders, i.e.

$$\frac{\partial u_0}{\partial t} = N(u_0, u_{0x}, u_{0xx}, \cdots, \mu)\,, \quad \text{(5a)}$$

$$\frac{\partial u_1}{\partial t} = L_1(u_0)u_1 + F_1(u_0)\,, \quad \text{(5b)}$$

$$\frac{\partial u_2}{\partial t} = L_2(u_0)u_2 + F_2(u_0,u_1)\,, \quad \text{(5c)}$$

$$\vdots$$

where the first equation is the $O(1)$ balance, the second equation is the $O(\epsilon)$ balance and the third equations is the $O(\epsilon^2)$ balance. As in the approach of Weinstein [34], we consider a solution of the leading order problem with slow-time modulation. Let $u_0(x,t)$ be given by

$$u_0(x,t) = \Phi(x,t,A_1,A_2,\cdots)\,, \quad \textbf{(6)}$$

where the parameters $A_i(\tau)$ vary with the slow time scale τ. Applying the Fredholm alternative to the forced, linear PDE for u_1 requires that the forcing term F_1 be orthogonal to the generalized null space of the adjoint operator $L_1^\dagger$, i.e. if $(L_1^\dagger)^m v = 0$ for some $m > 0$, then

$$\langle v, F_1\rangle = 0\,, \quad \textbf{(7)}$$

where $\langle u, v\rangle = \int_D uv^*\,dx$ is the inner product over the domain D. For a given perturbation, this constraint will result in equations for the slow evolution of the parameters A_i of the form

$$\frac{\partial A_i}{\partial \tau} = f_i(A_1, A_2, \cdots)\,. \quad \textbf{(8)}$$

Remarkably, in Weinstein's analysis of the NLSE [34], these constraints are all that needs to be satisfied to show that ϵu_1 is small for small values of ϵ up to times of order $1/\epsilon$. Similar results hold for elliptic function solutions of the NLSE, which we outline in the following. We will show that the additional terms in the LLE, when viewed as a perturbation of the NLSE, have a stabilizing effect on the parameters of dn type solutions. Further, we provide expressions for the evolution of the parameters for two particular cavity perturbations of the LLE: the Raman effect and spontaneous emission noise.

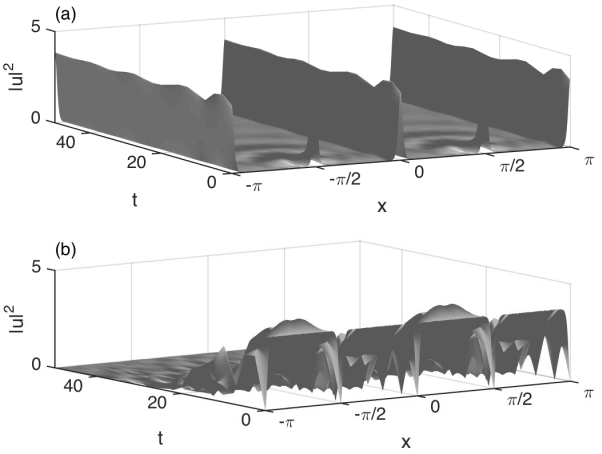

Fig. 1. Numerical simulation of the (a) cn and (b) sn solutions of Eq. (2) with $|\beta| = 0.01$, $\epsilon = 0.1$, $G = 0$, and the detuning α set to (a) $\alpha = 1.8732$ and (b) $\alpha = 3.7464$ (these values of the detuning are chosen so that $k^2 = 1 - 10^{-12} \approx 1$ in the analog of Eq. (11) for these solutions). The solutions were seeded with a white noise perturbation to induce instability in the evolution. Both solutions are unstable, even in the limit $k \to 1$ where the linear stability analysis shows the eigenvalues to shrink to the real axis. Note that the cn solution collapses from an $N = 4$ solution to a stable $N = 2$ dn solution.

JACOBI ELLIPTIC FUNCTIONS FOR THE NLSE

The Jacobi elliptic functions are periodic wavefunctions that satisfy the NLSE with detuning [28–31], i.e. the leading order dynamics as described by Eq. (2). The three basic functions are denoted $\mathrm{sn}(x|k)$, $\mathrm{cn}(x|k)$, and $\mathrm{dn}(x|k)$, where the elliptic modulus, k, parameterizes the solutions. The value of k is constrained such that $k \in [0, 1)$; we note that the reader may be more familiar with the parameter $m = k^2$, which is commonly used in software for evaluating the Jacobi elliptic functions.

The stability of these solutions is well-studied. For the defocusing case, the sn solutions are known to be modulationally stable [35]. For the focusing case, the cn and dn solutions are modulationally unstable [36]. Recent research has shown the spectral stability of the dn solution under perturbations with a period equal to the fundamental period, but not under perturbations with a period equal to a multiple of the fundamental period [37]. Spectral stability of the $\mathrm{cn}(x|k)$ solution only holds when $k \in (0, k_c)$ under perturbations with a period equal to the fundamental period, with $k_c \approx 0.908$ [37]. In-depth discussion of the stability properties of Jacobi elliptic function solutions of the NLSE can be found in [35–37].

With the addition of the LLE terms, i.e. the damping and forcing of the microresonator, the cn and sn solutions are unstable in their respective regimes. In Figure 1, we plot a numerical simulation of the evolution of cn and sn wave forms (with four pulses) governed by the LLE. The sn wave form quickly decays and the cn wave form evolves into a solution of dn type (with two pulses). It appears that the LLE does not support pulses that are separated by a node, i.e. those with a π phase change between neighboring pulses. In contrast with its instability as a solution of the NLSE, the dn type solutions of the LLE are in fact stable, even with multiple pulses in the cavity. We will show that this stability can be understood analytically and we will focus on the dn type solutions for the remainder of the manuscript.

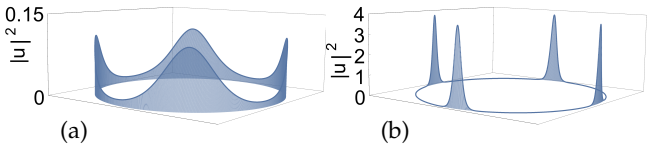

Fig. 2. The dn-type solutions for (a) $k^2 = 0.9$ and (b) $k^2 = 1 - 10^{-12} \approx 1$ with $N = 4$. The two panels demonstrate that the elliptic modulus $k \in [0, 1)$ can produce solutions which resemble a modulated CW beam or highly localized, hyperbolic secant pulses. Note that the dn solution has no nodal points where the solution is zero.

Solutions of dn type: anomalous dispersion

The dn solution is of the most practical importance, as it is the only stable solution we find for the LLE in the anomalous dispersion regime ($\beta < 0$). For this solution, we assume the general form

$$u_0(x,t) = \hat{u}_0 e^{i\psi} = A\,\mathrm{dn}(B(x - x_0)|k) e^{i[\xi(x-x_0)+\sigma-\sigma_0]}, \quad \textbf{(9)}$$

where $A^2 = -\beta B^2$, and

$$\frac{dx_0}{dt} = -\beta\xi, \quad (10a)$$

$$\frac{d\sigma}{dt} = -\alpha - \frac{\beta}{2}B^2(2 - k^2) - \frac{\beta}{2}\xi^2. \quad (10b)$$

Since the wavefunctions of the LLE should be $2\pi/N$ periodic, where N is a positive integer, the value of B determines the value of k and vice-versa. Specifically, the period of the Jacobi elliptic function $y = \mathrm{dn}(x|k)$ is $2K$, where $K(k)$ is the elliptic integral of the first kind. So the period of $\hat{u}_0 = \mathrm{dn}(Bx|k)$ should be $T = 2K/B$. If $T = 2\pi/N$, then we have $2K/B = 2\pi/N$, thus $B = KN/\pi$. Note that N is the number of localized (pulses) per round trip in the microresonator.

Figure 2 shows the dn solution for two values of the parameter k, where $k \in [0, 1)$. These figures are illustrated with $N = 4$ so that four pulses are shown around the cavity. In the limit $k \to 1$, the function $\mathrm{dn}(x|k) \to \mathrm{sech}(x)$, which is the standard hyperbolic secant soliton solution generated by the dominant NLSE terms. When $k \to 0$, the function $\mathrm{dn}(x|k) \to 1$, which is a continuous wave solution of the LLE. The figure illustrates the $k^2 = 0.9$ and $k^2 = 1 - 10^{-12} \approx 1$ solutions of the LLE. Figure 3 shows the dn solutions as the parameter N is varied from one to four.

Based on the observed behavior of these solutions of the LLE in numerical simulations, we consider solutions about the center frequency, $\xi = 0$, and with a fixed phase term, which can be obtained by setting

$$\alpha = -\beta B^2(2 - k^2)/2. \quad \textbf{(11)}$$

With these choices, the value of the detuning must be increased in order to accommodate more pulses per round trip, which is consistent with experimental findings.

Importantly, we can compute the cavity energy e_c versus detuning frequency α for the dn solutions by the definition of

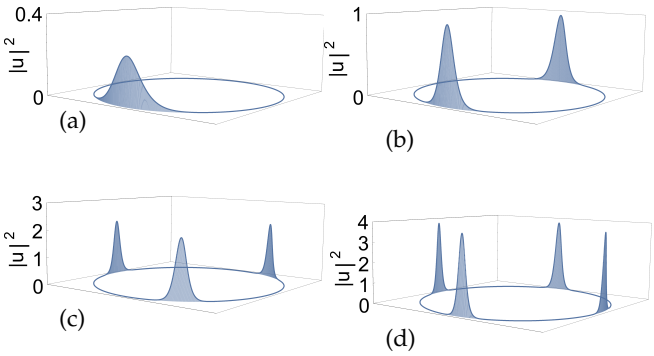

Fig. 3. The dn solution for $N = 1, 2, 3$ and 4. Here we plot dn solutions with the same modulus, $k^2 = 1 - 10^{-12} \approx 1$, as functions on a circle (to emphasize their periodicity). As the number of pulses N increases, the width of the each pulse narrows and the height increases. These four solution branches co-exist for a fixed value of the detuning α. The stability of each solution branch depends upon the detuning parameter as shown in Fig. 4.

the cavity energy as

$$e_c = \int_{-\pi}^{\pi} |u_0|^2 dx = -\beta B^2 \int_{-\pi}^{\pi} \mathrm{dn}^2(By|k) dy\,. \tag{12}$$

The energy of each solution branch can then be computed for different N values as shown in Fig. 4. The stability of each branch will be discussed in what follows, but the energy versus detuning shows the important trends to be considered. For $k \to 1$, the function $\mathrm{dn}(x|k) \to \mathrm{sech}(x)$ so that the energy integral can be approximated explicitly

$$e_c \approx -\beta B \int_{-B\pi}^{B\pi} \mathrm{sech}^2 z dz = -2\beta B\,. \tag{13}$$

Given that $\alpha \approx -\beta B^2/2$, we can then simplify the relationship between the detuning and cavity energy, i.e. $|e_c/\beta| \approx 2\sqrt{2}\sqrt{|\alpha/\beta|}$. This value is for only a single pulse. If there are N pulses, we obtain

$$|e_c/\beta| = 2\sqrt{2}N\sqrt{|\alpha/\beta|}. \tag{14}$$

This gives a simple quantization of the energy as a function of the number of pulses in the limit $k \to 1$. We will show in what follows that the $k \to 1$ limit is where solutions to the LLE are stable, thus the energy quantization formula is a good approximation for the LLE microresonator dynamics. Note that in Fig. 4, since $|\alpha/\beta| = B^2/2$, we have $|\alpha/\beta| \to \infty$ when $k \to 1$ and $|\alpha/\beta| \to 0$ when $k \to 0$.

STABILITY ANALYSIS OF THE LLE

The stability of the Jacobi elliptic function solutions to the LLE can be characterized using a linear stability analysis. Let $u_1 = e^{i\psi} w_1$. Following the perturbation expansion of Eq. (4), we find at leading order the Jacobi elliptic solutions and at $O(\epsilon)$ the linearized evolution

$$\hat{F} = i\frac{\partial w_1}{\partial t} - \alpha w_1 + 2|u_0|^2 w_1 - \frac{\beta}{2}\frac{\partial^2 w_1}{\partial x^2} + |u_0|^2 w_1^*\,, \tag{15}$$

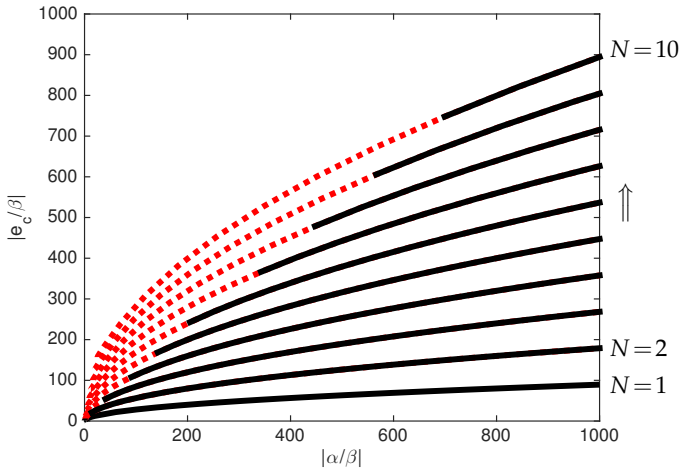

Fig. 4. The solution branches of the dn solution as a function of energy ($|e_c/\beta|$) versus detuning ($|\alpha/\beta|$). Plotted are the solution branches from $N = 1$ to $N = 10$. The instability of each branch can be computed from the linearized operator Eq. 17. Specifically, if the real part of any eigenvalue crosses the threshold of 5×10^{-4}, then the branch is considered unstable (dashed red lines) for that value of detuning. For candidate branches that are potentially stable (black lines), further analysis (as shown in Sec. 5) is required to confirm the stability of the dn solution branches. This figure matches recent experimental findings of [15] and confirms that the specific number of pulses in the microresonator can be controlled by manipulation of the detuning.

where $\hat{F} = i(e^{-i\psi}F + e^{-i\psi}G(u_0, x, t) - \hat{u}_0 - e^{-i\psi}u_{0\tau})$.

We can decompose the linearized evolution into real and imaginary components by letting $w_1 = R + iI$ ($w_1^* = R - iI$) so that in matrix notation it takes the form

$$\begin{bmatrix} R_t \\ I_t \end{bmatrix} = \begin{bmatrix} 0 & \frac{\beta}{2}\partial_x^2 - \hat{u}_0^2 + \alpha \\ -\frac{\beta}{2}\partial_x^2 + 3\hat{u}_0^2 - \alpha & 0 \end{bmatrix} \begin{bmatrix} R \\ I \end{bmatrix} + \begin{bmatrix} \mathrm{Im}\,\hat{F} \\ \mathrm{Re}\,\hat{F} \end{bmatrix}, \tag{16}$$

where ∂_x^2 denotes the second order derivative. The eigenvalue spectrum of the matrix in Eq. (16) yields the spectral stability of dn solutions, generally. Note that for $\hat{u}_0$ given by the dn solution, $\alpha = -\beta B^2(2 - k^2)/2$.

Figure 5 shows the computed spectrum of the linearized operator in Eq. (16) for the dn solution with $N = 4$. The operator was numerically evaluated using a spectrally accurate method with 1024 grid points (a fast Fourier transform was used to evaluate the second derivatives) and a standard matrix eigenvalue solver. The eigenvalues corresponding to both $k^2 = 0.9$ and $k^2 = 1 - 10^{-12} \approx 1$ are evaluated. Note for the case $N = 4$, the fundamental period $T = \frac{2\pi}{4}$, thus $[-\pi, \pi]$ is a multiple of the fundamental period, so we expect instability [37]. For $k^2 = 0.9$, the dn solution clearly has unstable eigenvalues, i.e. eigenvalues with large positive real part. As $k \to 1$, the real part of the eigenvalues of dn shrink to the imaginary axis, suggesting that the $k \to 1$ solutions will be better behaved, even if they are technically unstable [37]. Thus a critical part of the analysis is to determine if the addition of the LLE term F stabilizes such microresonator solutions subject to slow-time modulation of the parameters.

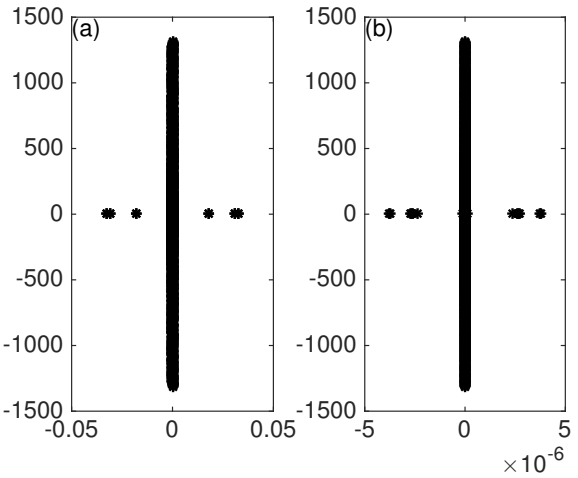

Fig. 5. Eigenvalue spectrum of the matrix $\mathbf{L}$ defined in Eq. (16) for the dn solution with (a) $k^2 = 0.9$ and (b) $k^2 = 1 - 10^{-12} \approx 1$. Although the eigenvalues shrink to the imaginary axis as $k \to 1$, the solutions are known to be unstable under generic perturbations.

Discrete Spectrum of dn Solutions

As with soliton perturbation theory, the generalized null space of the adjoint of the linearized operator is critical for determining stability. Specifically, the Fredholm-alternative theorem stated in Eq. (7) requires that perturbations be orthogonal to the null space of the adjoint linear operator (this removes so-called "secular" modes which have polynomial growth in time [34]). For the dn solution, the linear operator reduces to

$$\mathbf{L} = -\frac{\beta}{2}B^2 \begin{bmatrix} 0 & L_- \\ -L_+ & 0 \end{bmatrix}, \tag{17}$$

with the self-adjoint operators

$$L_- = -\frac{d^2}{dz^2} - 2\,\mathrm{dn}^2 z - k^2 + 2\,, \tag{18a}$$
$$L_+ = -\frac{d^2}{dz^2} - 6\,\mathrm{dn}^2 z - k^2 + 2\,, \tag{18b}$$

where a change of variables to $z = B(x - x_0)$ has been made and the dependence of dn on k has been dropped for notational convenience.

In the following, we will denote the generalized nullspace of a linear operator L by $\ker_g(L)$, i.e.

$$\ker_g(L) = \bigcup_{m=1}^{\infty} \ker(L^m)\,. \tag{19}$$

We also require the space $H^m_{\mathrm{per}}[a,b)$, which denotes a periodic Sobolev space on $[a,b)$. This space may be characterized by the Fourier coefficients of a given function. Let f be a function defined on $[a,b) = [-\pi,\pi)$ and let c_j defined by

$$c_j = \frac{1}{2\pi}\int_{-\pi}^{\pi} f(x)e^{-ijx}\,dx\,. \tag{20}$$

Then the $H^m_{\mathrm{per}}[-\pi,\pi)$ norm is defined by

$$\|f\|^2_{H^m_{\mathrm{per}}} = \sum_j |c_j|^2(1 + |j|^2 + \cdots |j|^{2m})\,. \tag{21}$$

Note that if $\|f\|_{H^m_{\mathrm{per}}} < \infty$, then the Fourier coefficients of the $(m-1)st$ derivative of f are absolutely summable so that $f^{(m-1)}$ is continuous as a periodic function on $[-\pi,\pi)$. The space H^m_{per} can be defined for other intervals by appropriate scaling.

Let $w_1 = R + iI$ as above. As in [34], we define the space

$$\mathcal{M} = H^1_{\mathrm{per}} \times H^1_{\mathrm{per}} \bigcap \left(\ker_g(\mathbf{L}^\dagger)\right)^\perp\,, \tag{22}$$

which is where we will constrain the evolution of $(R,I)^\intercal$. Note that the domain for z is $[-NK(k), NK(k))$. We also define the periodic functions $\phi(z)$ and $\varphi(z)$ to be

$$\phi(z) = (K(k)E(z,k) - E(k)z)\,\mathrm{dn}\,z - k^2K(k)\,\mathrm{sn}\,z\,\mathrm{cn}\,z, \tag{23a}$$
$$\varphi(z) = k^2\,\mathrm{cn}\,z\,\mathrm{sn}\,z(K(k)E(z,k) - E(k)z) + (E(k) - K(k))\,\mathrm{dn}\,z + k^2K(k)\,\mathrm{cn}^2\,z\,\mathrm{dn}\,z\,, \tag{23b}$$

where $E(z,k) = \int_0^z \mathrm{dn}^2\,y dy$ is the incomplete elliptic integral of the second kind, $E(k) = E(K(k),k)$ is the complete elliptic integral of the second kind, and $K(k)$ is as above. For the sake of compactness, we will often drop the dependence of $E(k)$ and $K(k)$ on the modulus k in the following. Note that $E(z,k)$ is odd, $\phi(z)$ is odd, and $\varphi(z)$ is even — the parity of functions simplifies much of the following analysis. A set of eigenfunctions that span $\ker_g(\mathbf{L}^\dagger)$ can then be computed from the following observations

$$L_-[\mathrm{dn}\,z] = 0, \tag{24a}$$
$$L_+[\mathrm{sn}\,z\,\mathrm{cn}\,z] = 0, \tag{24b}$$
$$L_+L_-\,[\phi(z)] = L_+[-2k^2E\,\mathrm{sn}\,z\,\mathrm{cn}\,z] = 0, \tag{24c}$$
$$L_-L_+\,[\varphi(z)] = L_-[2((k^2-2)E - 2(k^2-1)K)\,\mathrm{dn}\,z] = 0, \tag{24d}$$

These results are used to derive some important properties of the operators $\mathbf{L}^\dagger$, L_+, and L_-, which are summarized in propositions 1 and 2. Proofs are included in the appendix.

Proposition 1 *Assume $N \in \mathbb{N}$ and $0 < k < 1$. The operator L_- is non-negative and self-adjoint, with $\ker(L_-) = \mathrm{span}\{\mathrm{dn}\,z\}$. The operator L_+ is self-adjoint, with $\ker(L_+) = \mathrm{span}\{\mathrm{sn}\,z\,\mathrm{cn}\,z\}$.*

Proposition 2 *Assume $N \in \mathbb{N}$ and $0 < k < 1$ and let $(f,g)^\intercal \in H^1_{\mathrm{per}} \times H^1_{\mathrm{per}}$. If the following orthogonality relations hold*

$$\langle f, \mathrm{dn}\,z\rangle = 0\,, \tag{25a}$$
$$\langle f, \phi(z)\rangle = 0\,, \tag{25b}$$
$$\langle g, \mathrm{sn}\,z\,\mathrm{cn}\,z\rangle = 0\,, \tag{25c}$$
$$\langle g, \varphi(z)\rangle = 0\,, \tag{25d}$$

then $(f,g)^\intercal \in \mathcal{M}$.

Bounding the evolution of w_1 ($N = 1$)

Following the analysis of Weinstein [34], the evolution of the term $w_1 = R + iI$ is bounded by considering the function

$$Q(f,g) = -\frac{\beta}{2}B^2[\langle L_+f, f\rangle + \langle L_-g, g\rangle]\,, \tag{26}$$

which is a conserved quantity along the solution trajectory for w_1, i.e. $dQ(R,I)/dt = 0$. For $(R,I)^\intercal \in \mathcal{M}$, we have the following bound.

Proposition 3 *Assume $N = 1$. Let $w = R + iI \in \mathcal{M}$. Then there exist constants C_1 and C_2 such that*

$$C_1 \left(\|R\|^2_{H^1_{\text{per}}} + \|I\|^2_{H^1_{\text{per}}} \right) \leq Q(R, I) , \tag{27}$$

$$C_2 \left(\|R\|^2_{H^1_{\text{per}}} + \|I\|^2_{H^1_{\text{per}}} \right) \geq Q(R, I) . \tag{28}$$

This proposition is the primary result needed in our analysis: if the slow evolution of the parameters B, ξ, x_0, and σ is such that $(R(t), I(t))^\intercal \in \mathcal{M}$, then for any T_0 we have $\sup_{0 \leq t \leq T_0/\epsilon} \|\epsilon w_1(t)\|_{H^1_{\text{per}}} \to 0$ as $\epsilon \to 0$. See [34] for details. A proof of Proposition 3 based on a variational formulation can be found in [37]. A more classical proof modeled after [34] is provided in the appendix.

Modulation equations for the dn solution ($N = 1$)

For the dn solution,

$$\partial_\tau (\hat{u}_0) = \sqrt{-\beta} B_\tau \, \mathrm{dn}\, z + A \frac{dk}{dB} B_\tau \, \mathrm{dn}_k z + A[B_\tau (x - x_0) - B x_{0\tau}] \, \mathrm{dn}_z z . \tag{29}$$

We consider solutions with $k \to 1$, so that $dk/dB \approx 0$. Using this approximation, the above reduces to

$$\partial_\tau (\hat{u}_0) = \sqrt{-\beta} B_\tau \, \mathrm{dn}\, z - A k^2 \, \mathrm{sn}\, z \, \mathrm{cn}\, z \left(\frac{B_\tau}{B} z - B x_{0\tau} \right) , \tag{30}$$

so that

$$\partial_\tau (u_0) = e^{i\psi} \sqrt{-\beta} B_\tau \, \mathrm{dn}\, z - e^{i\psi} A k^2 \, \mathrm{sn}\, z \, \mathrm{cn}\, z \left(\frac{B_\tau}{B} z - B x_{0\tau} \right) + i \left(\xi_\tau \frac{z}{B} - \xi x_{0\tau} - \sigma_{0\tau} \right) e^{i\psi} A \, \mathrm{dn}\, z \tag{31}$$

This gives the following expression for the forcing term

$$\mathrm{Im}\, \hat{F} = F \cos\psi + \mathrm{Re}(e^{-i\psi} G) - \sqrt{-\beta} B_\tau \, \mathrm{dn}\, z - A \, \mathrm{dn}\, z + A k^2 \left(\frac{B_\tau}{B} z - B x_{0\tau} \right) \mathrm{sn}\, z \, \mathrm{cn}\, z, \tag{32}$$

$$\mathrm{Re}\, \hat{F} = F \sin\psi - \mathrm{Im}(e^{-i\psi} G) + \sqrt{-\beta} \xi_\tau z \, \mathrm{dn}\, z - (\xi x_{0\tau} + \sigma_{0\tau}) A \, \mathrm{dn}\, z . \tag{33}$$

To constrain the forcing term $(\mathrm{Im}\, \hat{F}, \mathrm{Re}\, \hat{F})^\intercal$ to be in $\mathcal{M}$, Proposition 2 implies the following constraints

$$\langle \mathrm{Im}\, \hat{F}, \mathrm{dn}\, z \rangle = 0, \tag{34a}$$

$$\langle \mathrm{Im}\, \hat{F}, \phi(z) \rangle = 0, \tag{34b}$$

$$\langle \mathrm{Re}\, \hat{F}, \mathrm{sn}\, z \, \mathrm{cn}\, z \rangle = 0, \tag{34c}$$

$$\langle \mathrm{Re}\, \hat{F}, \varphi(z) \rangle = 0. \tag{34d}$$

These constraints require the slow evolution of the parameters to satisfy the following system of differential equations

$$\frac{dB}{d\tau} = \frac{\langle \mathrm{Re}(e^{-i\psi} G) + F \cos\psi, \mathrm{dn}\, z \rangle - \sqrt{|\beta|} B \langle \mathrm{dn}\, z, \mathrm{dn}\, z \rangle}{\sqrt{|\beta|} (\langle \mathrm{dn}\, z, \mathrm{dn}\, z \rangle - k^2 \langle z \, \mathrm{sn}\, z \, \mathrm{cn}\, z, \mathrm{dn}\, z \rangle)} , \tag{35a}$$

$$\frac{dx_0}{d\tau} = \frac{\langle F \cos\psi + \mathrm{Re}(e^{-i\psi} G), \phi(z) \rangle}{\sqrt{|\beta|} B^2 k^2 \langle \mathrm{sn}\, z \, \mathrm{cn}\, z, \phi(z) \rangle} , \tag{35b}$$

$$\frac{d\xi}{d\tau} = -\frac{\langle F \sin\psi - \mathrm{Im}(e^{-i\psi} G), \mathrm{sn}\, z \, \mathrm{cn}\, z \rangle}{\sqrt{|\beta|} \langle z \, \mathrm{dn}\, z, \mathrm{sn}\, z \, \mathrm{cn}\, z \rangle} , \tag{35c}$$

$$\frac{d\sigma_0}{d\tau} + \xi \frac{dx_0}{d\tau} = \frac{\langle F \sin\psi - \mathrm{Im}(e^{-i\psi} G), \varphi(z) \rangle}{\sqrt{|\beta|} B \langle \mathrm{dn}\, z, \varphi(z) \rangle} , \tag{35d}$$

where $\psi = \xi z / B + \sigma - \sigma_0$. We can further simplify the equations above by applying trigonometric identities, we have

$$\frac{dB}{d\tau} = \frac{\langle \mathrm{Re}(e^{-i\psi} G), \mathrm{dn}\, z \rangle + F \cos(\sigma - \sigma_0) p_1(\xi)}{\sqrt{|\beta|} (q_1(k) - k^2 q_2(k))} - \frac{\sqrt{|\beta|} B \langle \mathrm{dn}\, z, \mathrm{dn}\, z \rangle}{\sqrt{|\beta|} (q_1(k) - k^2 q_2(k)} , \tag{36a}$$

$$\frac{dx_0}{d\tau} = \frac{\langle \mathrm{Re}(e^{-i\psi} G), \phi(z) \rangle - F \sin(\sigma - \sigma_0) p_2(\xi)}{\sqrt{|\beta|} B^2 k^2 q_3(k)} , \tag{36b}$$

$$\frac{d\xi}{d\tau} = \frac{\langle \mathrm{Im}(e^{-i\psi} G), \mathrm{sn}\, z \, \mathrm{cn}\, z \rangle - F \cos(\sigma - \sigma_0) p_3(\xi)}{\sqrt{|\beta|} q_2(k)} , \tag{36c}$$

$$\frac{d\sigma_0}{d\tau} + \xi \frac{dx_0}{d\tau} = \frac{F \sin(\sigma - \sigma_0) p_4(\xi) - \langle \mathrm{Im}(e^{-i\psi} G), \varphi(z) \rangle}{\sqrt{|\beta|} B q_4(k)} , \tag{36d}$$

where

$$p_1(\xi) = \langle \cos(\xi z / B), \mathrm{dn}\, z \rangle , \tag{37a}$$

$$p_2(\xi) = \langle \sin(\xi z / B), \phi(z) \rangle , \tag{37b}$$

$$p_3(\xi) = \langle \sin(\xi z / B), \mathrm{sn}\, z \, \mathrm{cn}\, z \rangle , \tag{37c}$$

$$p_4(\xi) = \langle \cos(\xi z / B), \varphi(z) \rangle , \tag{37d}$$

and

$$q_1(k) = \langle \mathrm{dn}\, z, \mathrm{dn}\, z \rangle \tag{38a}$$

$$q_2(k) = \langle z \, \mathrm{dn}\, z, \mathrm{sn}\, z \, \mathrm{cn}\, z \rangle \tag{38b}$$

$$q_3(k) = \langle \mathrm{sn}\, z \, \mathrm{cn}\, z, \phi(z) \rangle \tag{38c}$$

$$q_4(k) = \langle \mathrm{dn}\, z, \varphi(z) \rangle . \tag{38d}$$

In addition to these constraints, ξ should be an integer so that u_0 remains in H^1_{per}. Therefore the analysis is only rigorous when applied to perturbations for which $d\xi/d\tau = 0$, but we have found that the analysis provides insight in other cases.

Consider the stability of this system of differential equations around the center frequency, i.e. $\xi = 0$, so that $\psi = \sigma - \sigma_0$ and $p_2(\xi) = p_3(\xi) = 0$. For $k \approx 1$, we can approximate many of the inner products in the above expressions using the limiting forms of the Jacobi elliptic functions. We obtain the approximations $p_1(0) \approx \pi$, $p_4(0) \approx 0$, $q_1(k) \approx 2$, $q_2(k) \approx 1$, $q_3(k) \approx -1$, and $q_4(k) \approx 1$. With these approximations, the evolution equations simplify to

$$\frac{dB}{d\tau} = \frac{1}{\sqrt{|\beta|}} (\langle \mathrm{Re}(e^{-i\psi} G), \mathrm{dn}\, z \rangle + F\pi \cos(\sigma - \sigma_0)) - 2B , \tag{39a}$$

$$\frac{dx_0}{d\tau} = -\frac{\langle \mathrm{Re}(e^{-i\psi} G), \phi(z) \rangle}{\sqrt{|\beta|} B^2} , \tag{39b}$$

$$\frac{d\xi}{d\tau} = \frac{1}{\sqrt{|\beta|}} \langle \mathrm{Im}(e^{-i\psi} G), \mathrm{sn}\, z \, \mathrm{cn}\, z \rangle , \tag{39c}$$

$$\frac{d\sigma_0}{d\tau} + \xi \frac{dx_0}{d\tau} = -\frac{\langle \mathrm{Im}(e^{-i\psi} G), \varphi(z) \rangle}{\sqrt{|\beta|} B} . \tag{39d}$$

These slow evolution equations approximate the effect of a perturbation G on the microresonator comb.

Stability of dn solutions of the LLE ($N = 1$)

When the perturbation $G = 0$, the parameter evolution constraints Eq. (39) yield the following set of equations

$$\frac{dB}{d\tau} = \frac{F\pi\cos(\sigma-\sigma_0)}{\sqrt{|\beta|}} - 2B\,, \tag{40a}$$

$$\frac{dx_0}{d\tau} = 0\,, \tag{40b}$$

$$\frac{d\xi}{d\tau} = 0\,, \tag{40c}$$

$$\frac{d\sigma_0}{d\tau} + \xi\frac{dx_0}{d\tau} = 0\,, \tag{40d}$$

which gives the solution with $B = F\pi\cos(\sigma-\sigma_0)/(2\sqrt{|\beta|})$ as a steady-state attractor to the dynamics. Specifically, values of B larger and smaller than this exponentially decay back to the steady-state value. In addition, the fast time scale dynamics give

$$\frac{dx_0}{dt} = -\beta\xi, \tag{41a}$$

$$\frac{d\sigma}{dt} = -\alpha - \frac{\beta}{2}B^2(2-k^2) - \frac{\beta}{2}\xi^2. \tag{41b}$$

Integrating the constant σ_0 into the second equation and setting $\xi = 0$, i.e. we are working around the center frequency, then

$$\frac{d(\sigma-\sigma_0)}{dt} = -\alpha - \frac{\beta}{2}B^2(2-k^2). \tag{42}$$

Since the first solvability condition gives the steady-state $B = F\pi\cos(\sigma-\sigma_0)/(2\sqrt{-\beta})$, then

$$\frac{d(\sigma-\sigma_0)}{dt} = -\alpha + \frac{F^2\pi^2(2-k^2)}{8}\cos^2(\sigma-\sigma_0)\,, \tag{43}$$

and

$$\cos(\sigma-\sigma_0) = \frac{2B\sqrt{-\beta}}{F\pi}\,, \tag{44}$$

which gives the time-independent phase of the microresonator comb. Specifically, the real part of the solution is $u_0 = A\,\mathrm{dn}(B(x-x_0),k)\cos(\sigma-\sigma_0)$ and the imaginary part is $u_0 = A\,\mathrm{dn}(B(x-x_0),k)\sin(\sigma-\sigma_0)$.

These asymptotic results show that $B \neq 0$ provided $F > 0$. Moreover, the stable microresonator solution has a fixed phase relation which does not evolve in time. Simulations show that these two predictions are accurate representations of the dynamics. More than that, the prediction here shows them to be attractors for general initial conditions, which is again borne out by simulation.

The case $N > 1$ in practice

Proposition 1 states that the nullspaces of L_+ and L_- are each spanned by one function, for any positive number of pulses N. However, in simulations of finite precision, this mathematical truth is not observed for $k \approx 1$. Indeed, the discretizations of these operators are observed to have N eigenfunctions corresponding to a zero (to numerical precision) eigenvalue when $k \approx 1$. Intuitively, this results from the fact that the dn function is nearly zero between pulses for $k \approx 1$ so that the pulses are essentially decoupled. Indeed, the set of N shifted copies of the eigenfunctions for $N = 1$, i.e. individual pulses in each of $[-K,K),[K,3K),\ldots,[(2N-3)K,(2N-1)K)$, is seen to give a basis for these nullspaces, again to numerical precision.

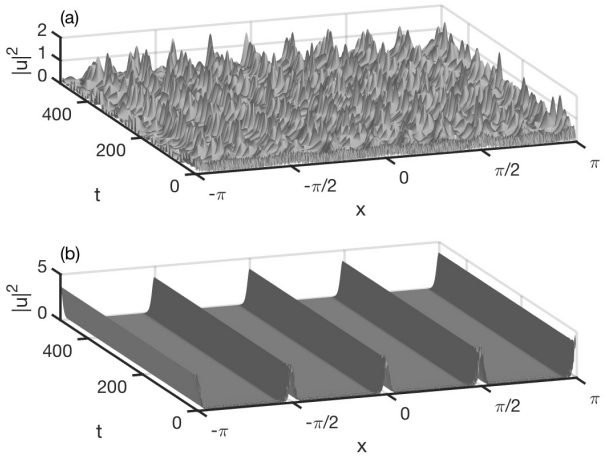

Fig. 6. Numerical simulation of the ($N = 4$) dn solution of Eq. (2) with $\epsilon = 0.1$, $G = 0$, and the detuning α set to (a) $\alpha = 0.0593$ and (b) $\alpha = 1.8732$ so that the appropriate parameter for the initial waveform is (a) $k^2 = 0.9$ and (b) $k^2 = 1-10^{-12} \approx 1$, according to Eq. (11). The initial waveform was corrupted with white noise to induce instability in the evolution. The $k^2 = 0.9$ solution is shown to be unstable whereas the $k^2 = 1-10^{-12}$ solution is stable. This is consistent with our linear stability analysis and Fig. 4.

Counterintuitively, it is this failure of Proposition 1 in practice which explains the predictive power of the modulation equations of the previous sections — which hold mathematically only when $N = 1$ — for numerical simulations with $N > 1$. In particular, for the LLE type perturbation alone ($G = 0$), we observe that the stabilizing effect on the amplitude of the comb as predicted by Eq. (40a) and the generation of a time independent phase as predicted by Eq. (44) for the $N = 1$ case also hold for $N > 1$ when $k \approx 1$. See Figures 6 and 7 for a comparison of the stability of a dn initial condition with and without the LLE terms, which we discuss in more detail in the next section. For nonzero G perturbations, as in the Raman effect and spontaneous emission noise examples below, the more qualitative $N = 1$ predictions are also observed numerically when $N > 1$. The fact that the behaviors of the pulses have decoupled is only apparent for the spontaneous emission noise example, as the perturbations acting on each pulse are identical in the other examples.

NUMERICAL SIMULATIONS

In this section, we compare numerical simulations of Eq. (2) with predictions made by the theory outlined above. In all simulations the value of β is fixed, with $\beta = -0.01$. When $\epsilon \neq 0$, we set $F = (\rho(1+(\rho-\alpha)^2))^{1/2}$ with $\rho = 0.95$ to remain in the right parameter space for the generation of frequency combs. The initial waveforms (u at time zero) are set according to Eq. (9) with $\xi = \sigma = \sigma_0 = x_0 = 0$ and the value of k determined by the detuning α as in Eq. (11). First, we simulate the LLE to show that the dn solution is stable, as opposed to the observed instability of the cn and sn solutions in Figure 1. Figure 6 shows the evolution of the dn solution for $\epsilon = 0.1$ and the detuning α chosen so that $k^2 = 0.9$ and $k^2 = 1-10^{-12} \approx 1$. Recall that for $k^2 = 0.9$ the linear stability analysis showed strong instability

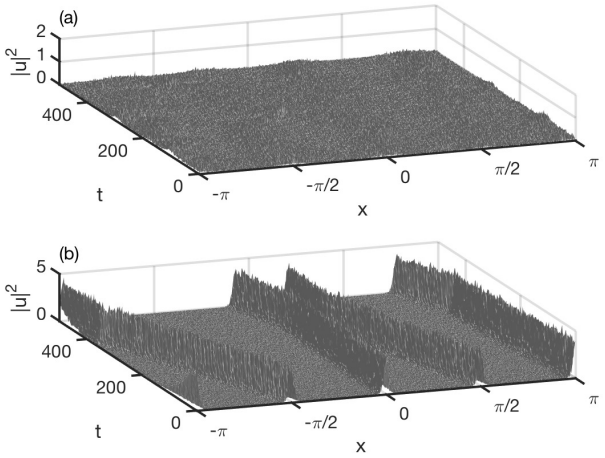

Fig. 7. Numerical simulation of the ($N = 4$) dn solution of Eq. (2) with $\epsilon = 0$, $G = 0$, and the detuning α set to (a) $\alpha = 0.0593$ and (b) $\alpha = 1.8732$ so that the appropriate parameter for the initial waveform is (a) $k^2 = 0.9$ and (b) $k^2 = 1 - 10^{-12} \approx 1$, according to Eq. (11). The initial waveform was corrupted with the same white noise as Fig. 6 to induce instability in the evolution. Both the $k^2 = 0.9$ solution and the $k^2 = 1 - 10^{-12}$ solution are unstable. Comparing with Fig. 6, we observe that the $k^2 = 1 - 10^{-12}$ solution is stabilized by the LLE type perturbation.

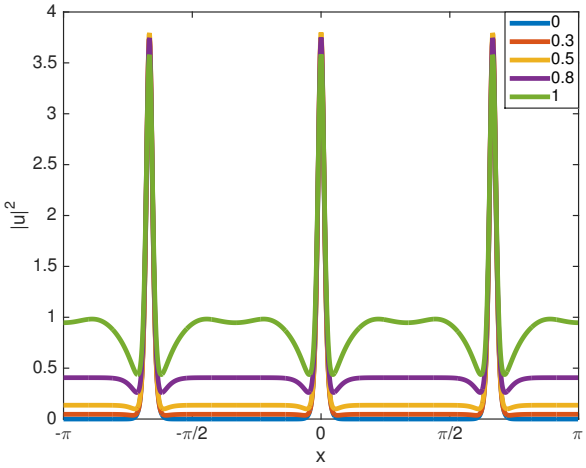

Fig. 8. Stable numerical solutions of Eq. (2) with $G = 0$ and $\alpha = 1.7793$ for various values of ϵ. The initial waveform was set as a ($N = 3$) dn solution with $k^2 = 1 - 10^{-16}$. As ϵ is increased from $\epsilon \ll 1$, the solutions deform from the asymptotic dn form to a localized structure that sits atop a shelf. Importantly, like the dn solution, the resulting evolution produces solutions which have no nodal separation between neighboring pulses.

and for $k^2 = 1 - 10^{-12}$ the analysis showed weaker instability, see Figure 5. Further, recall that for both values of the parameter, the solution should be unstable for generic perturbations of the equation. In both simulations, the initial waveforms are corrupted with white noise in order to induce instability if it exists. For $k^2 = 1 - 10^{-12}$, the pumping and damping terms of the LLE, i.e. the LLE-specific perturbations, have stabilized the dn solution. The $k^2 = 0.9$ solution is still unstable with this perturbation. In Fig. 7, we repeat these calculations without the LLE perturbation, i.e. setting $\epsilon = 0$. The $k^2 = 1 - 10^{-12}$ solution is seen to be less stable than that in Fig. 6.

In Fig. 8, we plot equilibrated solutions of Eq. (2) as ϵ is increased. In this example, the ($N = 3$) dn-type solutions for $k^2 = 1 - 10^{-16}$ remain stable, even for large values of ϵ. Note that the solutions deform away from the original dn waveform and develop a pedestal as ϵ is increased. Finally, Fig. 9 contains plots of the predicted time-independent phase, determined by Eq. (44), and the phase of a simulated microresonator solution with a dn initial waveform, showing good agreement between theory and simulation.

Raman term

An important modification to the LLE equation is the addition of the Raman effect which is known to induce a self-frequency shift in the microresonator [38, 39]. The Raman effect is included in the LLE as part of the perturbation term $G(u, x, t)$ in Eq. (2). Letting U denote the waveform and $\mathfrak{G}(U)$ denote the Raman perturbation in physical units, we have [38]

$$\mathfrak{G}(U) = i\left[-f_R|U|^2 + f_R h_R \bigotimes |U|^2\right] U \approx -i\left[f_R \tau_R \frac{\partial |U|^2}{\partial x}\right] U, \tag{45}$$

where the constants f_R and τ_R are the Raman fraction and the Raman shock time, respectively, and $\bigotimes$ denotes a convolution. In simulations, the Raman response function h_R is typically chosen to be [40]

$$h_R(x) = \frac{\tau_1^2 + \tau_2^2}{\tau_1 \tau_2^2} e^{-x/\tau_2} \sin(x/\tau_1), \tag{46}$$

where $\tau_1 = 12.2$fs and $\tau_2 = 32$fs. In our numerical simulation of the dimensionless LLE, Eq. (2), the Raman term becomes $G(u) = -iC\frac{\partial |u|^2}{\partial x} u$, where $C = 0.001$.

The effect of the Raman perturbation of Eq. (45) can be substituted into the modulation constraints of Eq. (39) to evaluate the impact on the comb dynamics. The symmetry properties of the perturbation play a large role in determining the resulting behavior. Specifically, symmetry considerations yield

$$\frac{dx_0}{d\tau} = 0\,, \tag{47a}$$

$$\frac{d\sigma_0}{d\tau} = 0\,, \tag{47b}$$

with the additional constraints that

$$\frac{dB}{d\tau} = \frac{F\pi \cos(\sigma - \sigma_0)}{\sqrt{-\beta}} - 2B\,, \tag{48a}$$

$$\frac{d\xi}{d\tau} = \frac{\langle 2CBA^3k^2\, \mathrm{dn}^2\, z\, \mathrm{sn}\, z\, \mathrm{cn}\, z, \mathrm{sn}\, z\, \mathrm{cn}\, z\rangle}{\sqrt{-\beta}} \neq 0 \tag{48b}$$

This determines the self-frequency shift induced by the Raman term since the value of ξ gives the shift from the center frequency used to derive the LLE. In addition to the self-frequency shift, it should be recalled that

$$\frac{dx_0}{dt} = -\beta\xi\,. \tag{49}$$

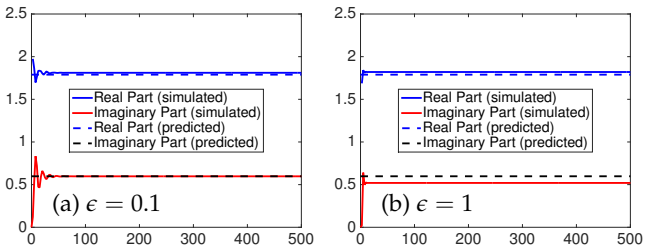

Fig. 9. Evolution of the real and imaginary parts of a ($N = 3$) dn solution of Eq. (2) evaluated at $x = 0$, with $G = 0$, $\alpha = 1.7793$ (so that the initial waveform has $k^2 = 1 - 10^{-16}$), and ϵ set to (a) $\epsilon = 0.1$ and (b) $\epsilon = 1$. The dotted lines are the theoretically calculated real and imaginary parts that result from our perturbation theory, whereas the solid lines are from the direct LLE simulation. The perturbation theory holds remarkably well even at $\epsilon = 1$.

As the term ξ is slowly evolving, it can be thought of as a constant over short time intervals so that the self-frequency shift generates a linear translation of the solution with a group velocity determined by the Raman term. Importantly, the Raman term does not destabilize the comb, rather it simply shifts it in frequency and forces a translation.

In Fig. 10, we plot simulations of the LLE with the addition of the Raman effect, i.e. $G(u) = -iC\frac{\partial|u|^2}{\partial x}u$, for both $\epsilon = 0.1$ and $\epsilon = 1$. The comb quickly forms and the induced translation is readily apparent. We also plot a line corresponding to the predicted drift velocity $dx_0/dt = -\beta\xi$. As noted above, only integer values of ξ are allowed by the model. Nonetheless, the frequency shift that ξ represents can be estimated from the simulation, and need not be integer valued. In particular, we take the empirical value of ξ to be the center of mass of the Fourier coefficients of the simulated waveform (computed using the FFT). After the first few time steps, this value holds steady at approximately $\xi = 0.3890$ for the $\epsilon = 0.1$ simulation and $\xi = 0.2608$ for the $\epsilon = 1$ simulation. The theoretical drift velocity matches well with the observed drift velocity of the simulation when $\epsilon = 0.1$, whereas, for $\epsilon = 1$, the prediction is not quantitatively satisfactory but corresponds to the qualitative behavior of the simulation (note that $\epsilon = 1$ is far from the asymptotic regime).

Spontaneous emission noise

Spontaneous emission noise from pumping/amplification has always been a significant source of performance limitations in optical systems. For instance, in optical communication systems, the noise from amplification results in the Gordon-Haus timing jitter [41] which imposes a fundamental limit on transmission lengths for a given bit-error-rate constraint in lightwave communication systems. Soliton perturbation theory provided the fundamental calculation of this limitation. It also provided a number of engineering design strategies for trying to overcome the Gordon-Haus limitations, including sliding filters [42, 43] and dispersion management [44–46].

The LLE perturbation theory developed here can also be used to evaluate the effects of spontaneous emission noise in the microresonator, something that has only recently been studied experimentally [47, 48]. Specifically, for this case the perturbation in Eq. (2) takes the form

$$G(u, x, t) = S(x, t)\,, \tag{50}$$

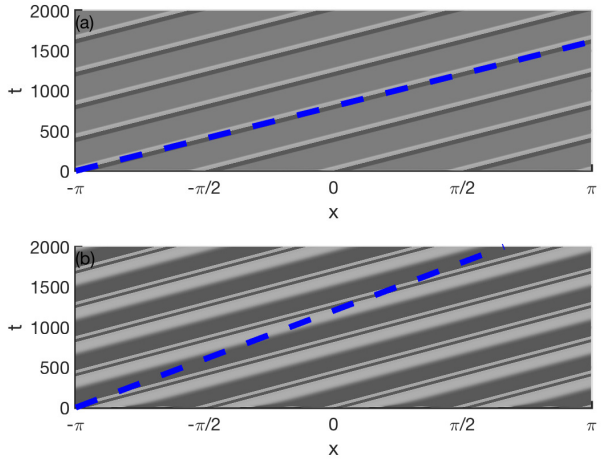

Fig. 10. Top view of a numerical simulation of Eq. (2) with $\alpha = 1.8732$ and the addition of the Raman effect of Eq. (45). The perturbation parameter ϵ is set to (a) $\epsilon = 0.1$ and (b) $\epsilon = 1$. As predicted and quantified by our perturbation theory, the dn solution remains stable despite the induced drift of the solution. The drift velocity is compared with that computed from our theory using self-frequency shift in both cases. The dotted lines represent the theoretically calculated trajectories of the drift of the solutions. The perturbation theory holds well when ϵ is small.

where $S(x, t)$ is a white noise process modeling the spontaneous emission [34]. In this case, for a specific realization of noise, the effects on the LLE comb parameters can be evaluated using Eq. (39). Generically, the noise generates amplitude, phase, center-position and center-frequency jitter. But the most pronounced effect comes from the fast scale dependency of the center position on the center frequency. Thus the evolution

$$\frac{d\xi}{d\tau} = \frac{1}{\sqrt{-\beta}}\left(\langle \mathrm{Re}(e^{-i\psi}S(x,t)), \mathrm{sn}\,z\,\mathrm{cn}\,z\rangle\right) \tag{51}$$

produces a center frequency with mean $\langle\xi\rangle$ and variance $\langle\xi^2\rangle$ which then drives the center position through the relation $dx_0/dt = -\beta\xi$. As with the Gordon-Haus jitter, this produces a jitter in the pulse position, leading to a degradation in performance. Figure 11 provides a simulation of the LLE under the influence of white noise perturbations Eq. (50). Note that the comb is stable, with fluctuations induced in the various solution parameters. Most notably, the zoom in of the individual pulses shows the random-walk generated as a result of the noise. As with Gordon-Haus jitter, the statistics of this random walk could be evaluated with the LLE perturbation theory we have developed.

CONCLUSIONS

In conclusion, we have shown that the LLE equation supports stable solutions of the Jacobi elliptic type. These solutions model periodic pulse trains of soliton-like solutions for which the pumping F is critical for stabilization. Our rigorous stability analysis also results in a perturbation theory for characterizing the effects of higher-order terms in the microresonator, such as may arise from Raman scattering, higher-order dispersion and spontaneous emission noise. The historical success of soliton

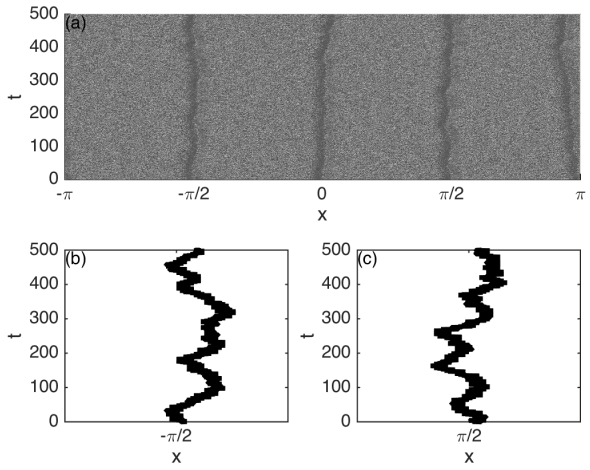

Fig. 11. (a) Top view of a numerical simulation of Eq. (2) with $\epsilon = 0.1$, $\alpha = 1.8732$, and the addition of spontaneous emission noise as defined in Eq. (50). As predicted and quantified by our perturbation theory, the dn solution remains stable despite the induced random walk (drift) of the individual pulse solutions. Much like the Gordon-Haus jitter, our perturbation theory captures the effect of the timing variance of individual pulses. To highlight the random walk of each pulse, panels (b) and (c) show a detail of the pulses near $x = -\pi/2$ and $x = \pi/2$ respectively.

perturbation theory in describing, for instance, Gordon-Haus timing jitter and/or the soliton self-frequency shifts, was critical in characterizing lightwave transmission systems and mode-locked lasers. Similarly, the LLE perturbation theory presented here can be a critically enabling tool for characterizing a host of additional microresonator phenomenon and potentially engineering new resonator designs with improved performance metrics.

Our stability analysis helps confirm several experimental observations. Most notably, it supports the recent observations that soliton states in the microresonator are not detuning degenerate, and can be individually addressed by laser detuning. Indeed, the theory rigorously confirms that the detuning can be used to lock the microresonator to any target multiple-pulse state, where the stability of each multiple-pulse state is explicitly computed and its minimum detuning assessed. The theory additionally shows that the phase-locking of the dn comb solution is an attractor to the resonator. Moreover, only solutions with no nodal separation (a zero separating pulses) are stabilized. Finally, the application of our theory to Raman scattering and stimulated emission perturbations show that neither effects destabilizes the comb. Rather, they both generate a drift in the pulse train, one which is deterministic in nature (Raman) and one which produces a random walk (noise).

ACKNOWLEDGMENTS

J. N. Kutz acknowledges support from the Air Force Office of Scientific Research (FA9550-17-1-0200). The authors would also like to thank the anonymous reviewers for their suggestions, which improved the quality of the analysis.

APPENDIX

In the following, we utilize some standard facts concerning the eigenvalues and zeros of Sturm-Liouville operators with periodic boundary conditions. See, for example, Theorem 3.1 of Chapter 8 in [49]. These arguments are modeled after those in [34].

Proof of Proposition 1

One can directly verify that $L_-[\mathrm{dn}\, z] = 0$. Because $\mathrm{dn}\, z$ has no zeros, $\lambda = 0$ is the first eigenvalue (listed in increasing order).

Again, one can verify that $L_+[\mathrm{sn}\, z\, \mathrm{cn}\, z] = 0$. There is at most one function (up to a constant multiple) in $\ker(L_+)$ which is linearly independent of $w(z) = \mathrm{sn}\, z\, \mathrm{cn}\, z$. Note that the natural domain for L_+ is $H^2_{\mathrm{per}}[0, 2NK)$ and recall that functions in H^2_{per} are determined by their values on $[0, 2NK)$ and periodicity. For integer j, we have that $w(jK) = 0$ and $w'(jK) = (-1)^j$. Suppose that v is another solution of $L_+[v] = 0$. We have that $w(z)v'(z) - w'(z)v(z)$ is constant, so that $(v/w)' = d/w^2$ for some constant d on any interval where $w \neq 0$. Consider an interval of the form $(jK, (j+1)K)$ and let $x_j = (j + 1/2)K$. For $jK < z < (j+1)K$, we have

$$v(z) = c_j w(z) + d_j w(z) \int_{x_j}^{z} \frac{dy}{w^2(y)} \,. \tag{52}$$

Let

$$\tilde{w}_j(z) = w(z) \int_{x_j}^{z} \frac{dy}{w^2(y)} \tag{53}$$

be defined on each interval $(jK, (j+1)K)$. It can be verified that the limit of $\tilde{w}_j(z)$ exists as you approach either endpoint. In particular, we have

$$\lim_{z \to 2jK^+} \tilde{w}_{2j}(z) = \lim_{z \to 2jK^-} \tilde{w}_{2j-1}(z) = -1 \,,$$
$$\lim_{z \to (2j+1)K^-} \tilde{w}_{2j}(z) = \lim_{z \to (2j+1)K^+} \tilde{w}_{2j+1}(z) = \frac{1}{\sqrt{1-k^2}} \,.$$

Because w is zero at all of these endpoints, we see that for v to be continuous, the d_j should all be equal. Without loss of generality, we set $d_j = 1$ for all j.

While the derivatives are still defined at the endpoints, they are not so well behaved. We have that

$$\begin{aligned} j_1 &:= \lim_{z \to 2jK^+} \tilde{w}'_{2j}(z) - \lim_{z \to 2jK^-} \tilde{w}'_{2j-1}(z) \\ &= \frac{2}{1-k^2} \left((1-k)^{3/2} - 1 + (2-k^2)E(K/2, k) - (1-k^2)K \right) \,, \\ j_2 &:= \lim_{z \to (2j+1)K^+} \tilde{w}'_{2j+1}(z) - \lim_{z \to (2j+1)K^-} \tilde{w}'_{2j}(z) \\ &= \sqrt{1-k^2} \left(j_1 - \frac{2(2-k^2)E - 4(1-k^2)K}{1-k^2} \right) \,. \end{aligned}$$

Note that, for $0 < k < 1$, $j_1 \neq j_2$. To enforce that v has continuous derivatives, we then obtain the following system of equations

$$
\begin{aligned}
c_1 - c_0 &= -j_1 \\
c_2 - c_1 &= j_2 \\
c_3 - c_2 &= -j_1 \\
&\vdots \\
c_{2N-1} - c_{2N-2} &= -j_1 \\
c_0 - c_{2N-1} &= j_2 \, .
\end{aligned}
$$

By summing all of the equations, we obtain that $0 = N(j_2 - j_1) \neq 0$, so that the equations are inconsistent. Therefore, there is no such v with a continuous derivative, i.e. there is no such v in $H^2_{\mathrm{per}}[0, 2NK)$. Note that for the case $k = 0$, we see that $j_1 = j_2$ so that such a v does exist, as expected.

Proof of Proposition 2

From Proposition 1, we have that

$$
\ker(\mathbf{L}^\dagger) = \mathrm{span}\{(\mathrm{dn}\, z, 0)^\intercal, (0, \mathrm{sn}\, z\, \mathrm{cn}\, z)^\intercal\} \, . \tag{54}
$$

Recall the definitions of ϕ and φ:

$$
\begin{aligned}
\phi(z) &= (KE(z,k) - Ez)\, \mathrm{dn}\, z - k^2\, \mathrm{sn}\, z\, \mathrm{cn}\, z, && \text{(55a)} \\
\varphi(z) &= k^2\, \mathrm{cn}\, z\, \mathrm{sn}\, z(KE(z,k) - Ez) + (E - K)\, \mathrm{dn}\, z \\
&\quad + k^2 K\, \mathrm{cn}^2\, z\, \mathrm{dn}\, z. && \text{(55b)}
\end{aligned}
$$

It can be verified that

$$
\begin{aligned}
L_+ L_-[\phi(z)] &= L_+\left[-2k^2 E\, \mathrm{sn}\, z\, \mathrm{cn}\, z\right] = 0, && \text{(56a)} \\
L_- L_+[\varphi(z)] &= L_-[2((k^2-2)E - 2(k^2-1)K)\, \mathrm{dn}\, z] = 0. && \text{(56b)}
\end{aligned}
$$

Therefore,

$$
\begin{aligned}
\ker((\mathbf{L}^\dagger)^2) = \mathrm{span}\{&(\mathrm{dn}\, z, 0)^\intercal, (0, \mathrm{sn}\, z\, \mathrm{cn}\, z)^\intercal, (\phi(z), 0)^\intercal, \\
&(0, \varphi(z))^\intercal\} \, .
\end{aligned} \tag{57}
$$

Suppose that $(f, g)^\intercal \in \ker((\mathbf{L}^\dagger)^3)$. Then, formally,

$$
\begin{aligned}
f &= c_1 L_-^{-1}\varphi(z) + c_2\phi(z) + c_3\, \mathrm{dn}\, z \, , && \text{(58)} \\
g &= c_4 L_+^{-1}\phi(z) + c_5\varphi(z) + c_6\, \mathrm{sn}\, z\, \mathrm{cn}\, z \, , && \text{(59)}
\end{aligned}
$$

where the inverses above denote a particular solution of the corresponding inhomogeneous ODE. Consider $L_-^{-1}\varphi(z)$. Note that the Fredholm alternative implies that

$$
\begin{aligned}
0 &= \langle k^2\, \mathrm{cn}\, z\, \mathrm{sn}\, z(KE(z,k) - Ez) + (E - K)\, \mathrm{dn}\, z, \mathrm{dn}\, z\rangle \\
&\quad + \langle k^2 K\, \mathrm{cn}^2\, z\, \mathrm{dn}\, z, \mathrm{dn}\, z\rangle && \text{(60)} \\
&= N(E^2 + (k^2-1)K^2) \, . && \text{(61)}
\end{aligned}
$$

For $0 < k < 1$, the expression $E^2 + (k^2-1)K^2 > 0$, a contradiction. Therefore, there is no such particular solution. Similarly, consider $L_+^{-1}\phi(z)$. The Fredholm alternative implies that

$$
\begin{aligned}
0 &= \langle (KE(z,k) - Ez)\, \mathrm{dn}\, z - k^2 K\, \mathrm{sn}\, z\, \mathrm{cn}\, z, \mathrm{sn}\, z\, \mathrm{cn}\, z\rangle && \text{(62)} \\
&= -\frac{N}{k^2}\left(E^2 + (k^2-1)K^2\right) \, , && \text{(63)}
\end{aligned}
$$

again, a contradiction. Therefore,

$$
\ker_g(\mathbf{L}^\dagger) = \ker((\mathbf{L}^\dagger)^2) \, . \tag{64}
$$

Proof of Proposition 3

The existence of C_2 is simple to establish. To establish the existence of C_1, we require the following two lemmas. Note that for the remainder of these statements, we assume that $N = 1$.

Lemma 1 *Suppose that $\langle f, \mathrm{dn}\, z\rangle = 0$ and $\langle f, \phi(z)\rangle$. Then there exists a positive constant C_1^+ such that*

$$
\langle L_+ f, f\rangle \geq C_1^+ \|f\|^2_{L^2} \, . \tag{65}
$$

Lemma 2 *Suppose that $\langle g, \mathrm{sn}\, z\, \mathrm{cn}\, z\rangle = 0$ and $\langle g, \varphi(z)\rangle = 0$. Then there exists a positive constant C_1^- such that*

$$
\langle L_- g, g\rangle \geq C_1^- \|g\|^2_{L^2} \, . \tag{66}
$$

Suppose that $\langle f, \mathrm{dn}\, z\rangle = 0$, $\langle f, \phi(z)\rangle$, $\langle g, \mathrm{sn}\, z\, \mathrm{cn}\, z\rangle = 0$, and $\langle g, \varphi(z)\rangle = 0$. Let C_1^+ and C_1^- be as in Lemmas 1 and 2, respectively. Then

$$
\begin{aligned}
&\langle L_+ f, f\rangle + 6\|f\|_{L^2} + \langle L_- g, g\rangle + 2\|g\|_{L^2} && \text{(67)} \\
&\quad = \|\frac{d}{dz} f\|_{L^2} + 6\langle (1 - \mathrm{dn}^2\, z) f, f\rangle + (2 - k^2)\|f\|_{L^2} && \text{(68)} \\
&\qquad + \|\frac{d}{dz} g\|_{L^2} + 2\langle (1 - \mathrm{dn}^2\, z) g, g\rangle + (2 - k^2)\|g\|_{L^2} \, , && \text{(69)} \\
&\quad \geq \|f\|_{H^1_{\mathrm{per}}} + \|g\|_{H^1_{\mathrm{per}}} \, . && \text{(70)}
\end{aligned}
$$

Therefore, the proposition holds with

$$
C_1 = \min\left(\frac{1}{1 + \frac{6}{C_1^+}}, \frac{1}{1 + \frac{2}{C_1^-}}\right) \, . \tag{71}
$$

Proof of Lemma 1

In the following, we repeat the argument of [34], making appropriate changes to handle the periodic case. First, we note that by Theorem 3.1 of Chapter 8 in [49], L_+ has one negative eigenvalue (when $N = 1$) with a corresponding eigenfunction f_0, which we take to be nonnegative without loss of generality. Define

$$
\gamma_1 = \min_f \langle L_+ f, f\rangle \, , \text{ where } \|f\|_2 = 1, \ \langle f, \mathrm{dn}\, z\rangle = 0 \, . \tag{72}
$$

Then, by Lemma E.1 of [34], we have that $\gamma_1 \geq 0$ if

$$
\langle L_+^{-1}\, \mathrm{dn}\, z, \mathrm{dn}\, z\rangle \leq 0 \, , \tag{73}
$$

which is straightforward to verify using arguments similar to those in the proof of Proposition 2. Therefore, $\gamma_1 \geq 0$. The lemma is then proved if we can show that $\gamma_2 = \inf_f \langle L_+ f, f\rangle$ with f restricted such that $\|f\|_{L^2} = 1$, $\langle f, \mathrm{dn}\, z\rangle = 0$, and $\langle f, \phi(z)\rangle = 0$ is non-zero, as $\gamma_2 \geq \gamma_1 \geq 0$.

Suppose that $\gamma_2 = 0$. Let f_m be a minimizing sequence of $\langle L_+ f, f\rangle$ satisfying $\|f_m\|_{L^2} = 1$, $\langle f_m, \mathrm{dn}\, z\rangle = 0$, and $\langle f_m, \phi(z)\rangle = 0$. Given $\delta > 0$, there exists a $M(\delta)$ such that

$$
\begin{aligned}
0 &< \int_{-K(k)}^{K(k)} \left(\frac{d}{dz} f_m\right)^2 dz + (2 - k^2) \int_{-K(k)}^{K(k)} f_m^2\, dz && \text{(74)} \\
&\leq 6 \int_{-K(k)}^{K(k)} \mathrm{dn}^2\, z f_m^2\, dz + \delta \, , && \text{(75)}
\end{aligned}
$$

for all $m \geq M(\delta)$. In particular, the sequence f_m is uniformly bounded in the H^1_{per} norm. Therefore, there is a subsequence of

f_m which converges weakly to an H^1_{per} function f_*. This function satisfies the constraints $\langle f_*, \mathrm{dn}\, z\rangle = 0$ and $\langle f_*, \phi(z)\rangle = 0$ by weak convergence. Because H^1_{per} is compactly embedded in L^2, there exists a further subsequence, which we denote by f_{m_j}, that converges in the L^2 norm (to f_*). Therefore, $\|f_*\|_{L^2} = 1$.

Let h be such that $\|h\|_2 = 1$. Note that $\langle h, f'_*\rangle = \lim\langle h, f'_{m_j}\rangle \leq \liminf \|f'_{m_j}\|_{L^2}$ by weak convergence in H^1_{per}. Taking the maximum over all such h implies that $\|f'_*\|_{L^2} \leq \liminf \|f'_{m_j}\|_{L^2}$. Combining this with the L^2 convergence of f_{m_j} gives that $\langle L_+ f_*, f_*\rangle \leq \liminf\langle L_+ f_{m_j}, f_{m_j}\rangle = 0$, so that $\langle L_+ f_*, f_*\rangle = 0$.

Because f_* attains the minimum and is admissible, there exists a critical point of the problem

$$(L_+ - \lambda_1) f = \lambda_2\, \mathrm{dn}\, z + \lambda_3 \phi(z)\,, \tag{76}$$

$$\|f\|_2 = 1\,, \tag{77}$$

$$\langle f, \mathrm{dn}\, z\rangle = 0\,, \tag{78}$$

$$\langle f, \phi(z)\rangle = 0\,, \tag{79}$$

of the form $(f_*, \lambda_1, \lambda_2, \lambda_3)$. Taking the inner product of f_* with Eq. (76), we obtain that $\lambda_1 = \langle L_+ f_*, f_*\rangle = 0$. This implies that

$$L_+ f_* = \lambda_2\, \mathrm{dn}\, z + \lambda_3 \phi(z)\,. \tag{80}$$

Taking the inner product of $\mathrm{sn}\, z\, \mathrm{cn}\, z$ with Eq. (80), we obtain that $\lambda_3 = 0$. Following the arguments in the proof of Proposition 2, this implies that

$$f_* = \frac{\lambda_2}{2((k^2-2)E - 2(k^2-1)K)}\varphi(z) + \lambda_4\, \mathrm{sn}\, z\, \mathrm{cn}\, z\,, \tag{81}$$

for some λ_4. The constraint $\langle f_*, \phi(z)\rangle = 0$ implies that $\lambda_4 = 0$ and the constraint $\langle f_*, \mathrm{dn}\, z\rangle = 0$ implies that $\lambda_2 = 0$. We have that $f_* \equiv 0$, a contradiction. Therefore, $\gamma_2 > 0$, proving the lemma.

Proof of Lemma 2

This lemma can be proved using arguments similar to the above.

REFERENCES

1. S. T. Cundiff and A. M. Weiner, "Optical arbitrary waveform generation," Nature Photonics **4**, 760–766 (2010).
2. T. J. Kippenberg, R. Holzwarth, and S. Diddams, "Microresonator-based optical frequency combs," Science **332**, 555–559 (2011).
3. P. DelHaye, T. Herr, E. Gavartin, M. Gorodetsky, R. Holzwarth, and T. J. Kippenberg, "Octave spanning tunable frequency comb from a microresonator," Physical Review Letters **107**, 063901 (2011).
4. S. B. Papp and S. A. Diddams, "Spectral and temporal characterization of a fused-quartz-microresonator optical frequency comb," Physical Review A **84**, 053833 (2011).
5. F. Ferdous, H. Miao, D. E. Leaird, K. Srinivasan, J. Wang, L. Chen, L. T. Varghese, and A. M. Weiner, "Spectral line-by-line pulse shaping of on-chip microresonator frequency combs," Nature Photonics **5**, 770–776 (2011).
6. J. Pfeifle, V. Brasch, M. Lauermann, Y. Yu, D. Wegner, T. Herr, K. Hartinger, P. Schindler, J. Li, D. Hillerkuss et al., "Coherent terabit communications with microresonator kerr frequency combs," Nature photonics **8**, 375–380 (2014).
7. W. Liang, D. Eliyahu, V. Ilchenko, A. Savchenkov, A. Matsko, D. Seidel, and L. Maleki, "High spectral purity kerr frequency comb radio frequency photonic oscillator," Nature communications **6** (2015).
8. M.-G. Suh, Q.-F. Yang, K. Y. Yang, X. Yi, and K. J. Vahala, "Microresonator soliton dual-comb spectroscopy," Science **354**, 600–603 (2016).
9. T. Herr, V. Brasch, J. Jost, C. Wang, N. Kondratiev, M. Gorodetsky, and T. Kippenberg, "Temporal solitons in optical microresonators," Nature Photonics **8**, 145–152 (2014).
10. X. Yi, Q.-F. Yang, K. Y. Yang, M.-G. Suh, and K. Vahala, "Soliton frequency comb at microwave rates in a high-q silica microresonator," Optica **2**, 1078–1085 (2015).
11. B. G. Bale, K. Kieu, J. N. Kutz, and F. Wise, "Transition dynamics for multi-pulsing in mode-locked lasers," Opt. Express **17**, 23137–23146 (2009).
12. M. O. Williams, E. Shlizerman, and J. N. Kutz, "The multi-pulsing transition in mode-locked lasers: a low-dimensional approach using waveguide arrays," J. Opt. Soc. Am. B **27**, 2471–2481 (2010).
13. F. Li, P. K. A. Wai, and J. N. Kutz, "Geometrical description of the onset of multi-pulsing in mode-locked laser cavities," J. Opt. Soc. Am. B **27**, 2068–2077 (2010).
14. T. Herr, V. Brasch, J. Jost, C. Wang, N. Kondratiev, M. Gorodetsky, and T. Kippenberg, "Temporal solitons in optical microresonators," Nature Photonics **8**, 145–152 (2014).
15. H. Guo, M. Karpov, E. Lucas, A. Kordts, M. H. Pfeiffer, V. Brasch, G. Lihachev, V. E. Lobanov, M. L. Gorodetsky, and T. J. Kippenberg, "Universal dynamics and deterministic switching of dissipative kerr solitons in optical microresonators," Nature Physics (2016).
16. L. A. Lugiato and R. Lefever, "Spatial dissipative structures in passive optical systems," Physical review letters **58**, 2209 (1987).
17. Y. K. Chembo and C. R. Menyuk, "Spatiotemporal lugiato-lefever formalism for kerr-comb generation in whispering-gallery-mode resonators," Phys. Rev. A **87**, 053852 (2013).
18. V. Karpman and E. Maslov, "Perturbation theory for solitons," JETP **73**, 537–559 (1977).
19. Y. Kodama and M. J. Ablowitz, "Perturbations of solitons and solitary waves," Studies in Applied Mathematics **64**, 225–245 (1981).
20. D. Kaup, "Perturbation theory for solitons in optical fibers," Physical Review A **42**, 5689 (1990).
21. J. Elgin, "Perturbations of optical solitons," Physical Review A **47**, 4331 (1993).
22. F. Kartner, I. Jung, and U. Keller, "Soliton mode-locking with saturable absorbers," IEEE Journal of Selected Topics in Quantum Electronics **2**, 540–556 (1996).
23. T. Kapitula, J. N. Kutz, and B. Sandstede, "Stability of pulses in the master mode-locking equation," JOSA B **19**, 740–746 (2002).
24. T. Kapitula, N. Kutz, and B. Sandstede, "The evans function for nonlocal equations," Indiana University mathematics journal pp. 1095–1126 (2004).
25. B. G. Bale and J. N. Kutz, "Variational method for mode-locked lasers," J. Opt. Soc. Am. B **25**, 1193–1202 (2008).
26. C. Godey, I. V. Balakireva, A. Coillet, and Y. K. Chembo, "Stability analysis of the spatiotemporal lugiato-lefever model for kerr optical frequency combs in the anomalous and normal dispersion regimes," Phys. Rev. A **89**, 063814 (2014).
27. M. C. Cross and P. C. Hohenberg, "Pattern formation outside of equilibrium," Reviews of modern physics **65**, 851 (1993).
28. L. D. Carr, C. W. Clark, and W. P. Reinhardt, "Stationary solutions of the one-dimensional nonlinear schrödinger equation. ii. case of attractive nonlinearity," Physical Review A **62**, 063611 (2000).
29. J. C. Bronski, L. D. Carr, B. Deconinck, and J. N. Kutz, "Bose-einstein condensates in standing waves: The cubic nonlinear schrödinger equation with a periodic potential," Physical Review Letters **86**, 1402 (2001).
30. J. C. Bronski, L. D. Carr, B. Deconinck, J. N. Kutz, and K. Promislow, "Stability of repulsive bose-einstein condensates in a periodic potential," Physical Review E **63**, 036612 (2001).
31. J. C. Bronski, L. D. Carr, R. Carretero-González, B. Deconinck, J. N. Kutz, and K. Promislow, "Stability of attractive bose-einstein condensates in a periodic potential," Physical Review E **64**, 056615 (2001).
32. C. M. Bender and S. A. Orszag, Advanced mathematical methods for scientists and engineers I: Asymptotic methods and perturbation theory (Springer Science & Business Media, 2013).
33. J. Kevorkian and J. D. Cole, Perturbation methods in applied mathematics, vol. 34 (Springer Science & Business Media, 2013).

34. M. I. Weinstein, "Modulational stability of ground states of nonlinear schrödinger equations," SIAM journal on mathematical analysis **16**, 472–491 (1985).
35. N. Bottman, B. Deconinck, and M. Nivala, "Elliptic solutions of the defocusing nls equation are stable," Journal of Physics A: Mathematical and Theoretical **44**, 285201 (2011).
36. B. Deconinck and B. L. Segal, "The stability spectrum for elliptic solutions to the focusing nls equation," Physica D: Nonlinear Phenomena **346**, 1–19 (2017).
37. S. Gustafson, S. Le Coz, and T.-P. Tsai, "Stability of periodic waves of 1d cubic nonlinear schrödinger equations," Applied Mathematics Research eXpress **2017**, 431–487 (2017).
38. M. Karpov, H. Guo, A. Kordts, V. Brasch, M. H. Pfeiffer, M. Zervas, M. Geiselmann, and T. J. Kippenberg, "Raman self-frequency shift of dissipative kerr solitons in an optical microresonator," Physical review letters **116**, 103902 (2016).
39. C. Milián, A. V. Gorbach, M. Taki, A. V. Yulin, and D. V. Skryabin, "Solitons and frequency combs in silica microring resonators: Interplay of the raman and higher-order dispersion effects," Physical Review A **92**, 033851 (2015).
40. K. J. Blow and D. Wood, "Theoretical description of transient stimulated raman scattering in optical fibers," IEEE Journal of Quantum Electronics **25**, 2665–2673 (1989).
41. J. P. Gordon and H. A. Haus, "Random walk of coherently amplified solitons in optical fiber transmission," Optics letters **11**, 665–667 (1986).
42. A. Mecozzi, J. D. Moores, H. A. Haus, and Y. Lai, "Soliton transmission control," Optics letters **16**, 1841–1843 (1991).
43. L. F. Mollenauer, J. P. Gordon, and S. G. Evangelides, "The sliding-frequency guiding filter: an improved form of soliton jitter control," Optics letters **17**, 1575–1577 (1992).
44. M. Suzuki, I. Morita, N. Edagawa, S. Yamamoto, H. Taga, and S. Akiba, "Reduction of gordon-haus timing jitter by periodic dispersion compensation in soliton transmission," Electronics Letters **31**, 2027–2029 (1995).
45. N. Smith, W. Forysiak, and N. Doran, "Reduced gordon-haus jitter due to enhanced power solitons in strongly dispersion managed systems," Electronics Letters **32**, 2085–2086 (1996).
46. J. N. Kutz and P. Wai, "Gordon-haus timing jitter reduction in dispersion-managed soliton communications," IEEE Photonics Technology Letters **10**, 702–704 (1998).
47. T. Herr, K. Hartinger, J. Riemensberger, C. Wang, E. Gavartin, R. Holzwarth, M. Gorodetsky, and T. Kippenberg, "Universal formation dynamics and noise of kerr-frequency combs in microresonators," Nature Photonics **6**, 480–487 (2012).
48. P. Liao, C. Bao, A. Kordts, M. Karpov, M. H. Pfeiffer, L. Zhang, A. Mohajerin-Ariaei, Y. Cao, A. Almaiman, M. Ziyadi et al., "Dependence of a microresonator kerr frequency comb on the pump linewidth," Optics Letters **42**, 779–782 (2017).
49. E. A. Coddington and N. Levinson, Theory of ordinary differential equations (Tata McGraw-Hill Education, 1955).